Revision 1

Local structure in *C2/c* clinopyroxenes on the hedenbergite ($CaFeSi_2O_6$)-ferrosilite ($Fe_2Si_2O_6$) join: A new interpretation for the Mössbauer spectra of Ca-rich *C2/c* clinopyroxenes

Yassir A. Abdu* and Frank C. Hawthorne

Department of Geological Sciences, University of Manitoba, Winnipeg, MB R3T 2N2, Canada

*E-mail: Yassir.Abdu@ad.umanitoba.ca

Abstract

Three synthetic Ca-rich clinopyroxenes on the hedenbergite-ferrosilite join, with compositions ($Hd_{50}Fs_{50}$), ($Hd_{60}Fs_{40}$), and ($Hd_{70}Fs_{30}$), were investigated by single-crystal X-ray diffraction and Mössbauer spectroscopy at room temperature. For all samples, there is no evidence for the presence of phases with symmetry other than *C2/c*. Structure refinement, using a split-atom model, shows the existence of two different local configurations in the M2 cavity, a hedenbergite-like arrangement and a *C2/c* clinoferrosilite-like arrangement that are centered by Ca and Fe^{2+}, respectively. The Mössbauer spectra were analyzed by a quadrupole-splitting-distribution (QSD) method, and the hyperfine parameters of the QSD fit indicate the presence of Fe^{2+} in three local environments that are similar to those of Fe^{2+} at the M1 site in hedenbergite, and the M1 and M2 sites in *C2/c* clinoferrosilite, in agreement with the structure-refinement results. Our results are consistent with the calculated phase diagram for hedenbergite-ferrosilite, where a miscibility gap and a two-metastable-clinopyroxene field (hedenbergite and pigeonite) occur at low temperature. The coexistence of a hedenbergite-like configuration around Ca and a *C2/c* clinoferrosilite-like configuration around Fe can be considered as a precursor for pyroxene exsolution at low temperature. Our results support previous structure-refinement work on Ca-rich clinopyroxenes along the diopside-enstatite join, and provide a new insight in the interpretation of Mössbauer spectra of Ca-rich *C2/c* clinopyroxenes.

Keywords: clinopyroxene, hedenbergite-ferrosilite, crystal structure, local structure, Mössbauer spectroscopy, X-ray diffraction.

Introduction

Pyroxene is an important rock-forming mineral in the Earth's upper mantle and one of the major constituents of stony meteorites. The study of pyroxenes and their chemistry is essential for determining the petrogenesis of their host rocks. Calcium pyroxenes along or near the join diopside($CaMgSi_2O_6$)-hedenbergite($CaFe^{2+}Si_2O_6$) are monoclinic and have space-group symmetry *C2/c*. The larger and the more distorted M2 polyhedron is usually occupied by Ca, and the M1 polyhedron contains Mg, Fe^{2+}, trivalent and tetravalent cations (Cameron and Papike 1980).

Mössbauer spectroscopy is one of the techniques that has been used extensively in the study of pyroxenes, with emphasis on Mg-Fe^{2+} order-disorder over the non-equivalent M1 and M2 sites (e.g. Dundon and Hafner 1971; Skogby et al. 1992; Domeneghetti and Steffen 1992; Dyar et al. 2007). The Mössbauer spectra of orthopyroxenes are generally simple, and consist of two overlapping doublets at room temperature (RT) due to Fe^{2+} at the M1 (outer doublet) and M2 (inner doublet) sites. However, the spectra of Ca-rich clinopyroxenes (space group *C2/c*) are more complicated, and their interpretation is more difficult. For example, where the RT spectra of Ca-rich *C2/c* clinopyroxenes, with a small Ca-deficiency at the M2 site, are fit with two doublets and assignment is made as above, the relative area of the M2 doublet is anomalously larger than that expected from stoichiometry (Williams et al. 1971), which results in overestimation of the amount of Fe^{2+} at the M2 site. Williams et al. (1971) observed these anomalies in the spectra of both natural and synthetic *C2/c* Ca-rich clinopyroxenes with a Ca deficiency at the M2 site. They postulated a fine-domain structure of two exsolved *C2/c* phases of different Ca content, and accordingly fitted the clinopyroxene spectra with three doublets: two doublets for Fe^{2+} at the M1 site, and one doublet for Fe^{2+} at the M2 site (assuming that the M2

doublets for the two phases are strongly overlapping and cannot be resolved). Similarly, Dowty and Lindsley (1973) assumed that more than one doublet is necessary to describe the absorption due to Fe^{2+} at the M1 site in intermediate synthetic clinopyroxenes along the hedenbergite-ferrosilite ($Fe_2Si_2O_6$) join. However, they suggested a different explanation involving variation in next-nearest-neighbour (NNN) configurations around the M1 site due to different arrangements of Fe^{2+} and Ca at the neighbouring M2 sites.

NNN effects were also proposed by Aldridge et al. (1978) to explain line broadening of the absorption from Fe^{2+} at the M1 site in sodic clinopyroxene, where the NNN cations at M2 are Ca and Na. Dollase and Gustafson (1982) studied the Mössbauer spectra of synthetic sodic clinopyroxenes along some binary joins, and used multiple doublets in fitting Fe^{2+} at M1. However, they interpreted their two-doublet fit to the M1 absorption in Ca-Na clinopyroxene as being due to two electronic orbital configurations of Fe^{2+} at M1. Recently, quadrupole-splitting distributions (QSD) methods, which are superior compared to discrete Lorentzian-doublet fits (Rancourt 1994), have provided better fits to the Mössbauer spectra of Ca-rich clinopyroxenes (Eeckhout and De Grave 2003; De Grave and Eeckhout 2003; Redhammer et al. 2006; Abdu et al. 2009). However, the spectral interpretations remain similar to the above-mentioned models.

X-ray crystal-structure analysis and determination of the M2 site occupancy in *C2/c* Ca-rich clinopyroxene (with Ca < 1 at M2) has also been a difficult task. The average structure refinement of these clinopyroxenes shows a residual electron-density peak in the difference-Fourier synthesis which is located at ~ 0.6 – 0.7 Å from the M2 site along the y-axis (the M2' site) and is occupied by Fe and/or Mg (Rossi et al. 1987; Bruno et al. 1982). The M2-M2' split site has been observed in synthetic and natural clinopyroxenes both with and without observable microstructures (Rossi et al. 1987). On the basis of the observed M2'–O bond lengths in synthetic

C2/c clinopyroxene along the diopside-enstatite ($Mg_2Si_2O_6$) join, the anion configuration around M2' (occupied by Mg) is a distorted square pyramid, similar to that coordinating the M2 site in *C2/c* $Zn_2Si_2O_6$, whereas Ca at M2 is [8]-coordinated, similar to that of diopside (Bruno et al. 1982). However, split-atom refinement for the O2 and O3 anions (Tribaudino et al. 1989), results in [6]-coordination for Mg at M2', similar to that in high-pigeonite (i.e. pigeonite with *C2/c* symmetry).

The phase relations along the join hedenbergite-ferrosilite are similar to those of diopside-enstatite (Lindsley 1983), and similar behaviour and local structural configurations are expected in the former. Ohashi et al. (1975) refined the crystal structures of some synthetic *C2/c* clinopyroxenes on the join hedenbergite-ferrosilite, which has also been studied by Mössbauer spectroscopy (Dowty and Lindsley 1973). However, their refinements did not consider split-atom models and gave only the average structures of these clinopyroxenes, resulting in large atom-displacement parameters at the M2, O2 and O3 sites (i.e. suggesting positional disorder). Here we study three synthetic *C2/c* clinopyroxenes along the hedenbergite-ferrosilite join by Mössbauer spectroscopy and single-crystal X-ray structure refinement in order to evaluate aspects of local structural arrangements and short-range order.

Experimental

Synthetic Ca-Fe clinopyroxenes of nominal compositions $Fs_{75}Wo_{25}$, $Fs_{70}Wo_{30}$, and $Fs_{65}Wo_{35}$, hereafter referred to as $Hd_{50}Fs_{50}$, $Hd_{60}Fs_{40}$ and $Hd_{70}Fs_{30}$, respectively, were kindly provided by Dr. Darby Dyar. They were synthesized at ~ 950 ˚C and 20 kbar (Dowty and Lindsley 1973; Turnock et al. 1973), because clinopyroxenes on the hedenbergite-ferrosilite join with

hedenbergite content < 80 mole% are not stable relative to fayalite + SiO_2 at low pressure (Lindsley and Munoz 1969).

Single-crystal X-ray diffraction data were collected with a Bruker D8 three-circle diffractometer equipped with a rotating-anode generator (MoKα radiation), multilayer optics and an APEX-II detector. X-ray diffraction intensities were collected up to 60° 2θ and unit-cell parameters (Table 1) were refined using least squares. An absorption correction was done using the program SADABS (Sheldrick 2008).

Electron-microprobe analysis (EMPA) was done using a CAMECA SX-100 electron microprobe operating in wavelength-dispersion mode with the following conditions: excitation voltage: 15 keV, specimen current: 20 nA, beam size: 1 μm. We tried to analyze the same crystals used for the collection of the X-ray diffraction data, but only the crystal of $Hd_{70}Fs_{30}$ survived the polishing procedure. For the $Hd_{50}Fs_{50}$ and $Hd_{60}Fs_{40}$ samples, we analyzed a few grains of each sample. The average compositions (Table 2) do not differ significantly from the nominal compositions.

Mössbauer spectroscopy measurements were done in transmission geometry at RT using a ^{57}Co(Rh) point source. For preparing the Mössbauer absorber, the clinopyroxene sample was mixed with sugar and ground in acetone. The mixture was then loaded into a 2mm inner-diameter sample-holder containing ~ 3 mg Fe/cm^2. The spectra were analyzed using a Voigt-based quadrupole-splitting distribution (QSD) method (Rancourt and Ping 1991). To account for thickness and/or instrumental broadening, the Lorentzian linewidth of the symmetrical elemental doublets of the QSD was allowed to vary during spectrum fitting (Rancourt 1994). The centre shift is given relative to α-Fe at RT.

Results

Optimization of the refinement procedure

In the refinement of site scattering, a key issue is the type(s) of scattering factor used for the refinement. The total scattering for an ionized species is more than that for a neutral species for anions, and the inverse for cations, and hence the types of scattering factors used will affect the total refined site-scattering, both through the scattering factors of the refined species and through the scattering factors of the non-refined species (commonly anions). Cooper et al. (2009) examined this issue for the structure of kornerupine, $XM_9T_5O_{21}$(OH,F) where X = □, Fe^{2+}, Mg; M = Al, Mg, Fe^{2+}, Fe^{3+}; T = Si, Al, B, in which the three tetrahedrally coordinated T sites are occupied by Si, Al and B. The site scattering at the partly occupied X site is in accord with that determined by EMPA and SIMS for refinement with an ionized scattering factor for oxygen, whereas the values determined using a neutral scattering factor for oxygen deviate from the values determined by EMPA–SIMS by ~1.1 *epfu* (electrons per formula unit; Hawthorne et al. 1995). Lussier et al. (2011) examined this issue for the refinement of Si and B site-populations in liddicoatite where ^{11}B and ^{27}Al Magic-Angle-Spinning Nuclear Magnetic Resonance spectroscopy had shown that, in these samples, there is no $^{[4]}B$ or $^{[4]}Al$, and showed that the most accurate results were obtained with an ionized scattering factor for oxygen. Accurate site-populations are of particular petrologic interest in pyroxenes, and this work on synthetic pyroxenes, with the absence of minor cations common in natural pyroxenes, provides an opportunity to check the refinement methodology for the approach that gives the most accurate results.

Site occupancies. To refine the M1 and M2 site-occupancies, we used the following combinations of scattering factors: (1) Ca^{o}, Fe^{o}, O^{o}; (2) Ca^{2+}, Fe^{2+}, O^{o}; (3) Ca^{o}, Fe^{o}, O^{2-}; (4) Ca^{2+}, Fe^{2+}, O^{2-}. Scattering factors for ionized and neutral species were used for oxygen (Azavant and Lichanot 1993) and cations (International Tables for Crystallography). Furthermore, we used three different models (as discussed below) for positional disorder of both cations and anions: [1] no splitting; [2] splitting of the M2 site; [3] splitting of the M2, O2 and O3 sites. We focused our attention on crystal $Hd_{50}Fs_{50}$ for a total of twelve different refinements, and then used the optimum refinement method on crystals $Hd_{60}Fs_{40}$ and $Hd_{70}Fs_{30}$. For all models, the M1 site was set as containing only Fe (presuming that Ca is too large to occur at M1), and the occupancy of ^{M1}Fe was refined. For model [1], with no splitting, the M2 site was set as containing both Fe and Ca with the same positional coordinates, and the amount of each was varied under the constraint of full occupancy. For models [2] and [3], $^{M2'}Fe$ and ^{M2}Ca had different positional coordinates, as first shown by Rossi et al. (1981, 1983, 1987), Bruno et al. (1982) and Dal Negro et al. (1982, 1983). In model [2], the anion sites were not split, whereas for model [3], the O2 and O3 anion sites each were split (Tribaudino et al. 1989), and the split-anion sites were allowed to refine with independent positional coordinates but identical occupancies and displacement parameters. The results of the site-occupancy refinements for crystal $Hd_{50}Fs_{50}$ are given in Table 3.

The results of electron-microprobe analysis indicate that $Hd_{50}Fs_{50}$ is of nominal composition. Hence M1 = Fe and M2 = 0.50 Fe + 0.50 Ca. Table 3 compares the refined site occupancies for different combinations of scattering curves with the known (nominal) occupancy of each site. The differences between the refined and nominal values are listed, together with the Student T statistic for each difference. For the M1 site-occupancy, the T statistic is ~7-9 for all refinements using the neutral O^{o} scattering factor, and inspection of Table 3 shows that the site

188 occupancies are not in accord with the ideal value of 1.00. For the M1 site-occupancy, the T
189 statistic is ~1-2 for all refinements using the ionized O^{2-} scattering factor and inspection of Table
190 3 shows that the site occupancies are in accord with the ideal value of 1.00. We see similar
191 behaviour for the refined site-occupancies for M2, a more accurate refinement where the ionized
192 O^{2-} scattering factor is used, provided that we use model [2] or [3] (Table 3). The results are very
193 similar for neutral versus ionized scattering factors for Ca and Fe. Model [2] seems to give more
194 accurate site-occupancies for M2, using the ionized O^{2-} scattering factor, Table 3, but it does not
195 account for the positional disorder of anions, considered in model [3], which is important for
196 determining the local structure in the M2 cavity (as will be discussed below). It is apparent that
197 the correct scaling of the results occurs where the ionized O^{2-} scattering factor (rather than the
198 neutral O^{o} scattering factor) is used. This result is in accord with the previous results on other
199 minerals by Cooper et al. (2009) and Lussier et al. (2011).
200
201 **Structure refinement**
202 The crystal structures of synthetic clinopyroxene crystals $Hd_{50}Fs_{50}$, $Hd_{60}Fs_{40}$, and $Hd_{70}Fs_{30}$
203 were refined in the space group *C2/c* using the SHELXTL Version 5.1 software (Sheldrick
204 2008). Using the no-splitting model, the refinement gave R_1 indices of 1.68, 3.08 and 2.43% for
205 $Hd_{50}Fs_{50}$, $Hd_{60}Fs_{40}$ and $Hd_{70}Fs_{30}$, respectively, and difference-Fourier synthesis showed a
206 residual electron-density peak at ~ 0.5-0.7 Å from the M2 site along the y-axis: the M2' site.
207 Additionally, the M2, O2, and O3 atoms showed positional disorder, indicated by the
208 comparatively large equivalent-displacement parameter, U_{eq}, which for a given composition
209 follows the trend $U_{eq}(M2) > U_{eq}(O2) > U_{eq}(O3)$, and they generally increase with increase of the
210 ferrosilite component (Fig. 1). Similar positional disorder at the M2, O2 and O3 sites and the

211 composition trend of the U_{eq} values have been observed in C2/c clinopyroxenes of similar
212 composition along the hedenbergite-ferrosilite join (Ohashi et al. 1975). Such positional disorder
213 could be due to short-range (local) structure that may be revealed when atom-split refinement is
214 used (Tribaudino et al. 1989). To account for the significant residual electron-density and
215 positional disorder, we used split sites for M2, O2 and O3. The M1 site was not split, because the
216 cations at this site are not significantly positionally disordered (Fig. 1). The M2 site was split into
217 M2 and M2', and the occupancies of the M2 and M2' sites were refined as Ca and Fe,
218 respectively, with the constraint that the sum of the occupancies at M2+M2' = 1. The O2 and O3
219 sites were each split into two subsites (O2' and O2") and (O3' and O3"), respectively, using as
220 initial atom coordinates those of the O-split refinement of $Di_{66}En_{34}$ (Tribaudino et al. 1989). For
221 each pair of split O-sites, the atom-displacement parameters were constrained to be the same, and
222 the occupancies of the O2' and O2" (and O3' and O3") to be equal for $Hd_{50}Fs_{50}$, 0.6 and 0.4 for
223 $Hd_{60}Fs_{40}$, and 0.7 and 0.3 for $Hd_{70}Fs_{30}$. Refinement of $Hd_{70}Fs_{30}$ with anisotropic-displacement
224 parameters for all atoms led to convergence with positive anisotropic-displacements for all split
225 atoms, whereas refinement of $Hd_{60}Fs_{60}$ and $Hd_{50}Fs_{50}$ with anisotropic-displacement parameters
226 for all atoms led to convergence with negative anisotropic-displacements for the split O3 anions.
227 For $Hd_{60}Fs_{60}$ and $Hd_{50}Fs_{50}$, using isotropic-displacement parameters for the split O3 anions gave
228 positive displacement parameters for the split O3 anion. The refined atom coordinates and
229 equivalent isotropic-displacement parameters are listed in Table 4. The equivalent isotropic-
230 displacement parameters for the M2, O2 and O3 atoms decreased significantly and are similar to
231 those of the other sites in the structures (Table 4).

232 **Local structure in the M2 cavity.** From the different sets of coordinates and bond lengths
233 involving O1, O2', O2", O3' and O3", two arrangements were selected that lead to [8]-

234 coordinated M2 and [6]-coordinated M2' polyhedra centered by Ca and Fe^{2+}, respectively. The
235 M2–O and M2'–O bond lengths are given in Table 5 for both (Ca^{o}, Fe^{o} and O^{o}) and (Ca^{o}, Fe^{o}
236 and O^{2-}) models, along with the M2–O bond lengths for hedenbergite (Redhammer et al. 2006),
237 high-temperature *C2/c* clinoferrosilite (Sueno et al. 1984), and a fictive *C2/c* clinoferrosilite
238 calculated by Hugh-Jones et al. (1994) by extrapolating the structural data of Cameron et al.
239 (1973) and Ohashi et al. (1975) on *C2/c* Ca-clinopyroxenes along the hedenbergite-ferrosilite
240 join. Inspection of the interatomic distances show that the local arrangement around M2 (= Ca) is
241 very similar to that around the M2 site in hedenbergite (Table 5), and that the local arrangement
242 around M2' (= Fe^{2+}) is very similar to that around the M2 site in *C*2/*c* clinoferrosilite (Table 5).
243 This similarity suggests that in the structures of synthetic *C2/c* $Hd_{50}Fs_{50}$, $Hd_{60}Fs_{40}$ and $Hd_{70}Fs_{30}$,
244 Ca at M2 assumes a local coordination similar to that of Ca in hedenbergite, and Fe^{2+} at M2' has
245 a local coordination similar to that of $^{M2}Fe^{2+}$ in *C2/c* clinoferrosilite.
246
247 **Mössbauer spectroscopy**
248 The Mössbauer spectra of the synthetic clinopyroxenes (Fig. 2) are fitted to a QSD model
249 having two generalized QSD sites, one for Fe^{2+} at the M1 site (with two Gaussian components,
250 denoted as $^{M1}Fe^{2+}$ and $^{M1'}Fe^{2+}$) and the other for Fe^{2+} at the M2 site (with only one Gaussian
251 component, denoted as $^{M2'}Fe^{2+}$). The Mössbauer parameters are summarized in Table 6. All
252 parameters were allowed to vary during the fitting procedure. Furthermore, for the QSD site of
253 Fe^{2+} at M1, the centre shift (CS) was linearly coupled to the quadrupole splitting (QS) by the
254 relation: $CS = \delta_0 + \delta_1 QS$, where δ_1 is the coupling parameter. For all Fe sites, the CS values are
255 characteristic of high-spin Fe^{2+} in octahedral coordination (Table 6).

The QSD curves for Fe^{2+} at M1 (Fig. 2) show bimodal character with two overlapping components centered at QS values of ~ 2.3 mm/s ($^{M1}Fe^{2+}$) and ~ 2.7 mm/s ($^{M1'}Fe^{2+}$). The QS of $^{M1}Fe^{2+}$ and $^{M1'}Fe^{2+}$ do not show significant variation with composition, whereas the QS of $^{M2'}Fe^{2+}$ seems to decrease with increase in the ferrosilite content (Table 6), which resulted in better resolution of spectra in that direction (Fig. 2). The $^{M1}Fe^{2+}$ component shows a larger Gaussian width, σ_{QS}, compared to $^{M1'}Fe^{2+}$, implying larger stereochemical variation around Fe^{2+} at the former site. The most noticeable result is the great similarity between the relative proportions of $^{M1}Fe^{2+}$ and $^{M1'}Fe^{2+}$ and the mole fractions of hedenbergite and ferrosilite, respectively (Table 6), for a given composition. In addition, $^{M1'}Fe^{2+}$ has nearly the same relative area as that of $^{M2'}Fe^{2+}$. This is most evident in $Hd_{50}Fs_{50}$ spectrum, where the M2' peaks are visually resolvable (Table 6). Recalling the structure-refinement results, and as there is no evidence for the presence of phases with symmetry other than *C2/c*, we may assign $^{M1}Fe^{2+}$ to a local environment similar to that of Fe^{2+} at the M1 site in hedenbergite, and $^{M1'}Fe^{2+}$ and $^{M2'}Fe^{2+}$ to two local environments similar to those of Fe^{2+} at the M1 and M2 sites, respectively, in *C2/c* clinoferrosilite.

The QS of $^{M1}Fe^{2+}$ (Table 6) is in close agreement with the QS values reported for Fe^{2+} at the M1 site in pure hedenbergite, QS = 2.24(1) mm/s (Dollase and Gustafson 1982); QS = 2.263(4) mm/s (Redhammer et al. 2006). The QS of $^{M1'}Fe^{2+}$ and $^{M2'}Fe^{2+}$ (Table 6) differ significantly from those of Fe^{2+} at the M1 and M2 sites, respectively, in orthoferrosilite [QS(M1) = 2.49(1) mm/s, QS(M2) = 1.906(4) mm/s (Dowty and Lindsley 1973); QS(M1) = 2.51(2) mm/s, QS(M2) = 1.92(2) mm/s (Dyar et al. 2007)] and $P2_1/c$ clinoferrosilite (QS(M1) = 2.609(5) mm/s, QS(M2) = 1.959(5) mm/s, McCammon and Tennant 1996). Thus, it is unlikely that $^{M1'}Fe^{2+}$ and $^{M2'}Fe^{2+}$ are due to exsolved orthoferrosilite or $P2_1/c$ clinoferrosilite. *C2/c* clinoferrosilite is stable only at high temperature (the transition from orthoferrosilite occurs at

1025 °C, Sueno et al. 1984) and/or high pressure (the transition from $P2_1/c$ clinoferrosilite occurs between 1.48 and 1.75 GPa at RT, Hugh-Jones et al. 1994). Therefore, no Mössbauer data are available at ambient conditions for comparison. However, we can compare our QS values for $^{M1'}Fe^{2+}$ and $^{M2'}Fe^{2+}$ with those extrapolated from the high-pressure data of McCammon and Tennant (1996) who studied synthetic $P2_1/c$ clinoferrosilite by high-pressure Mössbauer spectroscopy and observed a $P2_1/c$ to $C2/c$ transition between 1.33 and 1.74 GPa. This transition is characterized by a large increase in QS of Fe^{2+} at the M1 site and a small decrease in QS for Fe^{2+} at the M2 site (McCammon and Tennant 1996).

In Fig. 3, we reproduce the QS vs. pressure data of McCammon and Tennant (1996) for high-pressure $C2/c$ clinoferrosilite. McCammon and Tennant (1996) estimated QS values, at 0 GPa, of 2.90(1) and 1.87(1) mm/s for Fe^{2+} at the M1 and M2 sites, respectively, in $C2/c$ clinoferrosilite by extrapolating to zero pressure the data in the pressure range 1.74-3.84 GPa (dashed lines in Fig. 3). The estimated QS at 0 GPa for Fe^{2+} at the M2 site in $C2/c$ clinoferrosilite is in close agreement with the QS of $^{M2'}Fe^{2+}$ for $Hd_{70}Fs_{30}$, but that for Fe^{2+} at M1 is considerably larger than the QS of $^{M1'}Fe^{2+}$ for all samples (Table 6, Fig. 3). McCammon and Tennant (1996) considered the Mössbauer parameters at 1.40 and 1.54 GPa as representing a mixture of $P2_1/c$ and $C2/c$ phases, and these data were omitted from their regression analysis (dashed lines in Fig. 3). If we include these two data points and exclude the points at 1.74 GPa (if considered as outlier) and 3.84 GPa (has the same QS value as that at 2.90 GPa), we obtain a better correlation between QS and pressure for Fe^{2+} at the M1 site in high-pressure $C2/c$ clinoferrosilite ($r^2 = 0.70$, solid line in Fig. 3) that is statistically significant ($P = 0.037$). Extrapolation to zero pressure gives a QS of 2.71(1) mm/s that is in accord with our QS values for $^{M1'}Fe^{2+}$ (Table 6, Fig. 3). On the other hand, the correlation between QS and pressure for the M2 site in high-pressure $C2/c$

clinoferrosilite, when the 1.40 and 1.54 GPa data points are included ($r^2 = 0.94$, solid line in Fig. 3) is very similar to that of McCammon and Tennant (1996), hence we obtained a similar extrapolated QS value at 0 GPa (1.86(1) mm/s).

Assuming equal recoilless fractions for the different Fe sites, the Mössbauer relative areas for $^{M1}Fe^{2+}$, $^{M1'}Fe^{2+}$ and $^{M2'}Fe^{2+}$ (Table 6) correspond to $^{M1}Fe^{2+}$/Fe(total), $^{M1'}Fe^{2+}$/Fe(total) and $^{M2'}Fe^{2+}$/Fe(total) ratios, respectively. Using these ratios and the nominal total Fe, Fe^{2+} site occupancies were calculated and given in the last column of Table 6. The Fe^{2+} occupancies at the M2 site (M2') for $Hd_{50}Fs_{50}$, 0.48(3), $Hd_{60}Fs_{40}$, 0.35(3), and $Hd_{70}Fs_{30}$, 0.25(3), are in close agreement with the nominal occupancies (0.50, 0.40 and 0.30, respectively), particularly for $Hd_{50}Fs_{50}$ where the M2 peaks are well resolved (Fig. 2).

Discussion

Above, we showed that the optimum combination of scattering factors is Fe^o, Ca^o and O^{2-}. Figure 4 shows a comparison of the refinement results (M2-split model) versus the nominal site-occupancies for all three clinopyroxene compositions examined here. The M1 site is consistently occupied by Fe in all nominal compositions. As shown in Fig. 4a, the refined values for Fe^o, Ca^o and O^{2-} deviate from the nominal values by less than two standard deviations whereas the refined values for Fe^o, Ca^o and O^o deviate from the nominal values by several standard deviations. The M2 site is occupied by Ca and Fe. As all Ca must occur at the M2 site, the nominal Fe site-occupancies for all three compositions are equal to the Fs content of the clinopyroxene. As indicated in Fig. 4b, the refined values for Fe^o, Ca^o and O^{2-} deviate from the nominal values by less than two standard deviations whereas the refined values for Fe^o, Ca^o and O^o deviate from the

nominal values by several standard deviations. These results show that use of the O^{2-} scattering factor is essential if accurate site-occupancy results are to be obtained for pyroxenes.

Previous single-crystal X-ray structure refinement gave the average structures of synthetic *C2/c* clinopyroxenes along the hedenbergite-ferrosilite join and resulted in positional disorder, as indicated by large atom-displacement parameters at the M2, O2 and O3 sites (Ohashi et al. 1975). The cause of this positional disorder may be the existence of local structural arrangements which are not resolvable in the average structure. In this study, we used a split-atom model to account for positional disorder at the M2, O2 and O3 sites in synthetic *C2/c* $Hd_{50}Fs_{50}$, $Hd_{60}Fs_{40}$ and $Hd_{70}Fs_{30}$ clinopyroxenes. We observed two local configurations for the split M2 (Ca) and M2' (Fe) subsites; a hedenbergite-like and a *C2/c* clinoferrosilite-like configurations, respectively.

Our Mössbauer spectroscopic results are consistent with the structure-refinement data, and indicate that Fe^{2+} in these clinopyroxenes is present in three different local environments that are similar to Fe^{2+} at the M1 site in hedenbergite ($^{M1}Fe^{2+}$), and the M1 and M2 sites in *C2/c* clinoferrosilite ($^{M1'}Fe^{2+}$ and $^{M2'}Fe^{2+}$, respectively). The existence of hedenbergite-like and *C2/c* clinoferrosilite-like local arrangements in our synthetic clinopyroxenes is consistent with the calculated phase diagram at 1 atm for hedenbergite-ferrosilite (Lindsley 1969) where a miscibility gap and a two-metastable-clinopyroxene field (hedenbergite and pigeonite) occur below ~ 900 °C in clinopyroxene of intermediate composition. The coexistence of a hedenbergite-like arrangement for Ca and a *C2/c* clinoferrosilite-like arrangement for Fe could then be considered as a precursor for pyroxene exsolution at low temperature. As our clinopyroxenes were synthesized at ~ 20 kbar and 950 °C, i.e. in the stability field of *C2/c* clinoferrosilite, the *C2/c* clinoferrosilite-like configuration must have escaped the *C2/c—P2₁/c*

transition, which is displacive in nature, upon quenching to room temperature, due to the constraint of the surrounding hedenbergite-like structure.

Our results support the work of Tribaudino et al. (1989) who used an O-split model to refine the structures of synthetic *C2/c* $Di_{66}En_{34}$ and $Di_{80}En_{20}$ and found similar results for the local structure in the M2 cavity, a diopside-like arrangement around Ca and a *C2/c* clinoenstatite-like configuration for Mg. Our results extend this model to Ca-rich *C2/c* Ca-Fe-Mg clinopyroxenes that have crystallized above the solvus and quenched to room temperature. In this case, the two local arrangements are expected to be similar to a diopside-hedenbergite solid solution and a *C2/c* enstatite-ferrosilite solid solution, both having the same X_{Fe} [= Fe/(Fe+Mg)].

Dowty and Lindsley (1973) fitted the Mössbauer spectra of *C2/c* clinopyroxenes along the join hedenbergite-ferrosilite using four discrete Lorentzian doublets; the inner doublet was assigned to Fe^{2+} at M2 and the three outer doublets were assigned to Fe^{2+} at M1. They proposed that the peak broadening of Fe^{2+} at the M1 site is caused by the variation in NNN configurations around the M1 site as a result of different arrangements of Ca and Fe at the adjacent M2 site: (0Ca, 3Fe), (1Ca, 2Fe), (2Ca,1Fe) and (3Ca, 0Fe). For a given composition, the M1 doublets have similar CS but different QS values, and the QS for a given doublet varies with composition (Dowty and Lindsley 1973).

Contrary to the NNN model of Dowty and Lindsley (1973), our QSD fit to synthetic *C2/c* clinopyroxenes (which have similar compositions to those studied by Dowty and Lindsley (1973)) show that the absorption due to Fe^{2+} at M1 can adequately be modeled with only two QSD components that have average QS values of ~ 2.3 mm/s ($^{M1}Fe^{2+}$) and ~ 2.7 mm/s ($^{M1'}Fe^{2+}$). If the M1 site in pyroxene is located on the positive slope of the relation of the reduction function to distortion from perfect octahedral coordination (Ingalls 1964; Dowty and Lindsley 1973), then

the larger QS of $^{M1'}Fe^{2+}$ (the *C2/c* clinoferrosilite-like arrangement) compared to that of $^{M1}Fe^{2+}$ (the hedenbergite-like arrangement) may suggest a more distorted octahedral environment around Fe in the former. This is in accord with the X-ray structure refinements which show that the M1 octahedron in *C2/c* clinoferrosilite (Sueno et al. 1984) is more distorted than the M1 octahedron in hedenbergite (Redhammer et al. 2006). Thus we would expect that the QS of $^{M1}Fe^{2+}$ to be more temperature dependent than that of $^{M1'}Fe^{2+}$, which would result in increased overlap between them at low temperature. On the other hand, the M2 peaks would become more resolved at low temperature.

Future work using in-situ variable-temperature single-crystal X-ray diffraction and Mössbauer spectroscopy would help monitor positional disorder and the associated local structures in these clinopyroxenes, thus, allowing for further discussion of our results with previously published Mössbauer and structure refinement work on Ca-rich clinopyroxenes.

Acknowledgments

We thank Darby Dyar, along with Donald Lindsley and Alan Turnock, for providing the clinopyroxene samples (that are a subset of the samples of her much larger study currently in progress). This work was supported by a Canada Research Chair in Crystallography and Mineralogy to FCH, and Discovery, Major Equipment and Major Facilities Access grants from the Natural Sciences and Engineering Research Council of Canada, and Innovation grants from the Canada Foundation for Innovation. We also thank Mark Cooper and Ravinder Sidhu for the collection of X-ray diffraction and electron-microprobe data, respectively.

References cited

Abdu, Y.A., Scorzelli, R.B., Varela, M.E., Kurat, G., Souza Azevedo, I., Stewart, S.J., and Hawthorne, F.C. (2009) Druse clinopyroxene in D'Orbigny angritic meteorite studied by single-crystal X-ray diffraction, electron microprobe analysis and Mössbauer spectroscopy. Meteoritics and Planetary Science, 44, 581-587.

Aldridge, L.P., Bancroft, G.M., Fleet, M.E., and Herzberg, C.T. (1978) Omphacites studies, II. Mössbauer spectra of *C2/c* and *P2/n* omphacites. American Mineralogist, 63, 1107-1115.

Azavant, P. and Lichanot, A. (1993) X-ray scattering factors of oxygen and sulfur ions: an *ab initio* Hartree–Fock calculation. Acta Crystallographica, A49, 91-97.

Bancroft, G.M., Williams, P.G.L., and Burns, R.G. (1971) Mössbauer spectra of minerals along the diopside-hedenbergite tie line. American Mineralogist, 56, 1617-1625.

Bruno, E., Carbonin, S., and Molin, G. (1982) Crystal structure of Ca-rich clinopyroxenes on the $CaMgSi_2O_6$–$Mg_2Si_2O_6$ join. Tschermaks Mineralogische und Petrographische Mitteilungen, 29, 223-240.

Cameron, M., Sueno, S., Prewit, C.T., and Papike, J.J. (1973) High-temperature crystal chemistry of acmite, diopside, hedenbergite, jadeite, spodumene and ureyite. American Mineralogist, 58, 594-618.

Cameron, M. and Papike, J.J. (1980) Crystal chemistry of silicate pyroxenes. In C.T. Prewitt, Ed., Pyroxenes, p. 1-92. Reviews in Mineralogy, Mineralogical Society of America, Washington, D.C.

Cooper, M.A., Hawthorne, F.C., and Grew, E.S. (2009) The crystal chemistry of the kornerupine-prismatine series. I. Crystal structure and site populations. Canadian Mineralogist, 47, 233-262.

Dal Negro, A., Carbonin, S., Molin, G.M., Cundari, A., and Piccirillo, E.M. (1982) Intracrystalline cation distribution in natural clinopyroxenes of tholeiitic, transitional and alkaline basaltic rocks. In S.K. Saxena, Ed., Advances in Physical Geochemistry, Vol. 2, p. 117-150. Springer, New York, NY.

Dal Negro, A., Carbonin, S., Domeneghetti, M.C., Molin, G.M., Cundari, A., and Piccirillo, E.M. (1984) Crystal-chemistry and evolution of the clinopyroxenes in a suite of high pressure ultramafic nodules from the Newer Volcanics of Victoria, Australia. Contributions to Mineralogy and Petrology, 86, 221-229.

De Grave, E. and Eechhout, S.G. (2003) ^{57}Fe Mössbauer-effect studies of Ca-rich, Fe-bearing clinopyroxenes: Part III. Diopside. American Mineralogist, 88, 1145-1152.

Dollase, W.A. and Gustafson, W.I. (1982) ^{57}Fe Mössbauer spectral analysis of the sodic clinopyroxenes. American Mineralogist, 67, 311-327.

Domeneghetti, M.C. and Steffen, G. (1992) M1, M2 site populations and distortion parameters in synthetic orthopyroxenes from Mössbauer spectra and X-ray structure refinements. Physics and Chemistry of Minerals, 19, 298-306.

Dowty, E. and Lindsley, D.H. (1973) Mössbauer spectra of synthetic hedenbergite-ferrosilite pyroxenes. American Mineralogist, 58, 850-868.

Dundon, R.W. and Hafner, S.S. (1971) Cation disorder in shocked orthopyroxenes. Science, 174, 581-583.

Dyar, M.D., Klima, R.L., Lindsley, D., and Pieters, C.M. (2007) Effects of differential recoil-free fraction on ordering and site occupancies in Mössbauer spectroscopy of orthopyroxenes. American Mineralogist, 92, 424-428.

Eechhout, S.G. and De Grave, E. (2003) ^{57}Fe Mössbauer-effect studies of Ca-rich, Fe-bearing clinopyroxenes: Part I. Paramagnetic spectra of magnesian hedenbergite. American Mineralogist, 88, 1129-1137.

Hawthorne, F.C., Ungaretti, L., and Oberti, R. (1995) Site populations in minerals: terminology and presentation of results of crystal-structure refinement. Canadian Mineralogist, 33, 907-911.

Hugh-Jones, D.A., Woodland, A.B., and Angel, R.J. (1994) The structure of high-pressure *C2/c* ferrosilite and crystal chemistry of high-pressure *C2/c* pyroxenes. American Mineralogist, 79, 1032-1041.

Ingalls, R. (1964) Electric-field gradient tensor in ferrous compounds. Physical Review, 133, A787-A795.

International Tables for Crystallography (1992). Vol. C. Kluwer Academic Publishers, Dordrecht, The Netherlands.

Lindsley, D.H. and Munoz, J.L. (1969) Subsolidus relations along the join hedenbergite-ferrosilite. American Journal of Science, 267A (Schairer Volume), 295-324.

Lindsley, D.H. (1983) Pyroxene thermometry. American Mineralogist, 68, 477-493.

Lussier, A., Abdu, Y., Hawthorne, F.C., Michaelis, V.K., Aguiar, P.M., and Kroeker, S. (2011) Oscillatory zoned liddicoatite from Anjanabonoina, central Madagascar. I. Crystal chemistry and structure by SREF and ^{11}B and ^{27}Al MAS NMR spectroscopy. Canadian Mineralogist, 49, 63-88.

McCammon, C.A. and Tennant, C. (1996) High-pressure Mössbauer study of synthetic clinoferrosilite, FeSiO3. In M.D. Dyar, C. McCammon, and M.W. Schaefer, Eds., Mineral

Spectroscopy: A tribute to Roger G. Burns, p. 281-288. The Geochemical Society, Special Publication No. 5.

Ohashi, Y., Burnham, C.W., and Finger, L.W. (1975) The effect of Ca-Fe substitution on the clinopyroxene crystal structure. American Mineralogist, 60, 423-434.

Rancourt, D.G. and Ping, J.Y. (1991) Voigt-based methods for arbitrary-shape static hyperfine parameter distributions in Mössbauer spectroscopy. Nuclear Instruments and Methods in Physics Research, B58, 85-97.

Rancourt, D.G. (1994) Mössbauer spectroscopy of minerals. I. Inadequacy of Lorentzian-line doublets in fitting spectra arising from quadrupole splitting distributions. Physics and Chemistry of Minerals, 21, 244-249.

Redhammer, G.J., Amthauer, G., Roth, G., Tippelt, G., and Lottermoser, W. (2006) Single-crystal X-ray diffraction and temperature dependent ^{57}Fe Mössbauer spectroscopy on the hedenbergite-aegirine $(Ca,Na)(Fe^{2+},Fe^{3+})Si_2O_6$ solid solution. American Mineralogist, 91, 1271-1292.

Rossi, G., Tazzoli, V., and Ungaretti, L. (1981) Crystal-chemical studies on sodic clinopyroxenes. Proceedings of XI General Meeting I.M.A. Rock-forming minerals, p. 20-45.

Rossi, G., Smith, D.C., Ungaretti, L., and Domeneghetti, M.C. (1983) Crystal chemistry and cation ordering in the system diopside-jadeite: a detailed study by crystal structure refinement. Contributions to Mineralogy and Petrology, 83, 247-258.

Rossi, G., Oberti, R., Dal Negro, A., Molin, G.M., and Mellini, M. (1987) Residual electron density at the M2 site in *C2/c* clinopyroxenes: Relationships with bulk chemistry and sub-solidus evolution. Physics and Chemistry of Minerals, 14, 514-520.

Sheldrick, G.M. (2008) A short history of SHELX. Acta Crystallographica, A64, 112-122.

Skogby, H., Annersten, H., Domeneghetti, M.C., Molin, G.M., and Tazzoli, V. (1992) Iron distribution in orthopyroxene: A comparison of Mössbauer spectroscopy and X-ray refinement results. European Journal of Mineralogy, 4, 441-452.

Sueno, S., Kimata, M., and Prewitt, C.T. (1984) The crystal structure of high clinoferrosilite. American Mineralogist, 69, 264-269.

Tribaudino, M., Benna, P., and Bruno, E. (1989) Average structure and M2 site configurations in *C2/c* clinopyroxenes along the Di-En join. Contributions to Mineralogy and Petrology, 103, 452-456.

Turnock, A.C., Lindsley, D.H., and Grover, J.E. (1973) Synthesis and unit cell parameters of Ca-Mg-Fe pyroxenes. American Mineralogist, 58, 50-59.

Williams, P.G.L., Bancroft, G.M., Brown, M.G., and Turnock, A.C. (1971) Anomalous Mössbauer spectra of C2/c clinopyroxenes. Nature Physical Science, 230, 149-151.

497
498

499 **Figure captions**

500 Fig. 1. Variation of the equivalent-displacement parameter (U_{eq}) with composition for synthetic
501 *C2/c* clinopyroxenes (no-splitting model). Error bars are smaller than symbol when not visible.

502

503 Fig. 2. Room-temperature Mössbauer spectra of synthetic *C2/c* clinopyroxenes. Solid
504 subspectrum: Fe^{2+} at the M1 site, for which the QSD profile is shown on the right; dashed
505 subspectrum: Fe^{2+} at the M2 site. Residuals are shown above each spectrum.

506

507 Fig. 3. Variation of QS with pressure for high-pressure *C2/c* clinoferrosilite (data are from
508 McCammon and Tennant 1996). The dashed and solid lines are linear least-square fits by
509 McCammon and Tennant (1996) and this study, respectively, to estimate the QS at 0 GPa for
510 Fe^{2+} at the M1 (open squares) and M2 (filled squares) sites in *C2/c* clinoferrosilite. The filled and
511 open circles are the QS of $^{M1'}Fe^{2+}$ and $^{M2'}Fe^{2+}$, respectively, in our synthetic *C2/c* clinopyroxenes,
512 see text. Error bars for the QS are the same size as the symbols.

513

514 Fig. 4. Comparison of Fe site-occupancies (M2-split model) refined with the X-ray scattering
515 curves Fe^{o}, Ca^{o} and O^{o}(circles) and Fe^{o}, Ca^{o} and O^{2-} (squares) with the nominal site-occupancies
516 for synthetic clinopyroxenes $Hd_{50}Fs_{50}$, $Hd_{60}Fs_{40}$ and $Hd_{70}Fs_{30}$. (a) M1 site; (b) M2 site. The
517 vertical bars show ±1 standard deviation; for M2, the standard deviations are the same size as the
518 symbols when not visible.

519

520

521

522

523

Table 1. Crystallographic data and structure-refinement information for synthetic clinopyroxenes.

	$Hd_{50}Fs_{50}$	$Hd_{60}Fs_{40}$	$Hd_{70}Fs_{30}$
a (Å)	9.793(4)	9.806(4)	9.819(4)
b (Å)	9.078(4)	9.068(4)	9.056(3)
c (Å)	5.238(2)	5.238(2)	5.242(2)
β (°)	106.27(1)	105.92(1)	105.61(1)
V (Å^3)	447.1(5)	447.9(6)	449.0(5)
Space group	*C2/c*	*C2/c*	*C2/c*
Z	2	2	2
Crystal size (μm)	30 (spheroid)	5 × 15 × 20	20 × 40 × 60
Radiation/filter	Mo*Kα* (wavelength = 0.7107 Å)/graphite		
Unique reflections	660	658	662
Reflections $\|F_o\| > 4\sigma F$	616	493	629

524
525
526
527

528

Table 2. Average chemical composition (wt.%) and unit formula (*apfu*), normalized to 6 oxygen atoms, for synthetic clinopyroxenes.

	$Fs_{75}Wo_{25}$ ($Hd_{50}Fs_{50}$)	$Fs_{70}Wo_{30}$ ($Hd_{60}Fs_{40}$)	$Fs_{65}Wo_{35}$ ($Hd_{70}Fs_{30}$)
No. of spots	10	10	8
SiO_2	47.20(36)	46.87(24)	47.60(47)
Al_2O_3	0.00	0.04	0.02
Cr_2O_3	0.01	0.00	0.00
FeO	42.09(64)	40(1)	35.97(37)
MnO	0.02	0.02	0.01
MgO	0.00	0.00	0.00
CaO	11.11(48)	12.95(96)	16.10(9)
NiO	0.01	0.01	0.00
Total	100.43	99.92	99.70
Si	2.00(2)	1.99(1)	2.00(2)
Fe	1.49(2)	1.42(4)	1.27(1)
Ca	0.51(2)	0.59(4)	0.730(4)
Fs (%)	74.5 ± 1.4	70.6 ± 2.8	63.5 ± 0.6
Wo (%)	25.5 ± 1.1	29.4 ± 2.2	36.5 ± 0.3

529

530
531
532

Table 3. Site-occupancies in $Hd_{50}Fs_{50}$ synthetic clinopyroxene refined with neutral and ionized scattering factors.

No Splitting	R_1 (%)	M1	$^{M1}\Delta$	^{M1}t*	M2	$^{M2}\Delta$	^{M2}t
Ca^0, Fe^0, O^0	1.87	0.978(3)	0.022	7.3	0.481(3) Fe 0.519 Ca	0.019	6.3
Ca^{2+}, Fe^{2+}, O^0	1.90	0.980(3)	0.020	6.7	0.488(3) 0.512	0.012	4.0
Ca^0, Fe^0, O^{2-}	1.68	1.005(3)	0.005	1.7	0.553(3) 0.447	0.053	17.7
Ca^{2+}, Fe^{2+}, O^{2-}	1.75	1.006(3)	0.006	2.0	0.558(3) 0.442	0.058	19.3
M2 Split	R_1 (%)	M1	$^{M1}\Delta$	^{M1}t	M2+M2'	$^{M2}\Delta$	^{M2}t
Ca^0, Fe^0, O^0	1.61	0.982(2)	0.018	9.0	0.470(5) Fe 0.530 Ca	0.030	6.0
Ca^{2+}, Fe^{2+}, O^0	1.65	0.982(2)	0.018	9.0	0.470(5) 0.530	0.030	6.0
Ca^0, Fe^0, O^{2-}	1.41	1.002(2)	0.002	1.0	0.504(5) 0.496	0.004	0.8
Ca^{2+}, Fe^{2+}, O^{2-}	1.46	1.002(2)	0.002	1.0	0.505(6) 0.495	0.005	0.8
M2, O2, O3 Split	R_1 (%)	M1	$^{M1}\Delta$	^{M1}t	M2+M2'	$^{M2}\Delta$	^{M2}t
Ca^0, Fe^0, O^0	1.59	0.983(2)	0.017	8.5	0.472(5) Fe 0.528 Ca	0.028	5.6
Ca^{2+}, Fe^{2+}, O^0	1.63	0.983(2)	0.017	8.5	0.472(5) 0.528	0.028	5.6
Ca^0, Fe^0, O^{2-}	1.42	1.003(2)	0.003	1.0	0.509(6) 0.491	0.009	1.5
Ca^{2+}, Fe^{2+}, O^{2-}	1.49	1.004(2)	0.004	1.3	0.511(6) 0.489	0.011	1.8

$R_1 = \Sigma||F_o| - |F_c|| / \Sigma|F_o|$, where F_o and F_c are the observed and calculated structure factors.
Δ = difference between refined and nominal site occupancy.
*t-statistic.

533
534

535
536
537

Table 4. Atom coordinates and isotropic-displacement parameters ($Å^2$) for synthetic clinopyroxenes (split-M2-O2-O3 model).

Atom	x	y	z	U_{eq}
		$Hd_{50}Fs_{50}$		
T	0.29328(4)	0.08959(4)	0.24272(7)	0.00871(11)
M1	0	0.90516(3)	¼	0.00920(10)
M2	0	0.2976(3)	¼	0.0125(4)
M2'	0	0.2630(3)	¼	0.0125(4)
O1	0.12169(10)	0.08959(10)	0.1535(2)	0.0103(2)
O2'	0.3606 (15)	0.2463(18)	0.320(2)	0.0106(11)
O2''	0.3806(15)	0.2372(18)	0.373(2)	0.0106(11)
O3'	0.3520(3)	0.0136(3)	0.0042(6)	0.0082(3)
O3''	0.3511(3)	0.0394(3)	-0.0115(6)	0.0082 (3)
		$Hd_{60}Fs_{40}$		
T	0.29196(8)	0.09056(9)	0.23993(15)	0.0094(2)
M1	0	0.90567(7)	¼	0.0100(2)
M2	0	0.3000(6)	¼	0.0118(8)
M2'	0	0.2632(7)	¼	0.0118(8)
O1	0.1215(2)	0.0898(2)	0.1534(4)	0.0107(4)
O2'	0.361(2)	0.252(2)	0.323(3)	0.0092(16)
O2''	0.380(3)	0.229(3)	0.367(5)	0.0092(16)
O3'	0.3492(10)	0.03938(9)	-0.0142(18)	0.0085(6)
O3''	0.3522(7)	0.0149(5)	0.0015(12)	0.0085(6)
		$Hd_{70}Fs_{30}$		
T	0.29077(4)	0.09098(3)	0.23797(7)	0.00819(11)
M1	0	0.90619(2)	¼	0.00886(10)
M2	0	0.2998(2)	¼	0.0103(2)
M2'	0	0.2627(3)	¼	0.0103(2)
O1	0.12074(10)	0.08997(9)	0.1530(2)	0.0096(2)
O2'	0.3614(4)	0.2468(5)	0.3202(5)	0.0099(5)
O2''	0.3808(11)	0.2370 (13)	0.3745 (17)	0.0099(5)
O3'	0.362(3)	0.019(4)	0.011(6)	0.0103(8)
O3''	0.3463(11)	0.0246(17)	-0.011(2)	0.0103(8)

538
539
540

541
542

Table 5. M2–O and M2'–O bond lengths (Å) for synthetic clinopyroxenes (split-M2-O2-O3 model) refined with scattering factors (Fe^o, Ca^o and O^o) and (Fe^o, Ca^o and O^{2-}) (see text for details).

	Fe^o, Ca^o and O^o			Fe^o, Ca^o and O^{2-}			[1]Hd	[2]HT	[3]Fictive
	$Hd_{50}Fs_{50}$	$Hd_{60}Fs_{40}$	$Hd_{70}Fs_{30}$	$Hd_{50}Fs_{50}$	$Hd_{60}Fs_{40}$	$Hd_{70}Fs_{30}$		*C2/c* Fs	*C2/c* Fs
M2–O1 ×2	2.356(3)	2.358(6)	2.355(2)	2.362(3)	2.375(5)	2.366(2)	2.358(1)	-	-
M2–O2 ×2	2.31(1)	2.322(13)	2.333(2)	2.317(8)	2.324(13)	2.336(2)	2.339(1)	-	-
M2–O3 ×2	2.66(2)	2.64(2)	2.69(2)	2.626(3)	2.776(7)	2.681(12)	2.628(1)	-	-
M2–O3 ×2	2.80(1)	2.75(2)	2.71(5)	2.775(4)	2.774(9)	2.72(4)	2.720(1)	-	-
<M2–O>	2.532	2.518	2.522	2.520	2.562	2.526	2.511		
M2'–O1 ×2	2.107(3)	2.106(6)	2.097(3)	2.119(3)	2.117(5)	2.106(2)	-	2.161(15)	2.10(1)
M2'–O2 ×2	2.00(1)	2.02(3)	2.00(1)	1.994(9)	2.03(3)	2.001(8)	-	2.016(9)	2.005(5)
M2'–O3 ×2	2.80(1)	2.78(4)	2.82(4)	2.809(4)	2.822(7)	2.81(3)	-	2.722(13)	2.91(3)
M2'–O3 ×2	[3.07(1)]	[3.01(2)]	[2.94(2)]	[3.012(4)]	[3.04(1)]	[2.93(2)]	-	[3.191(13)]	[3.00(3)]
<M2'–O>	2.302	2.302	2.306	2.307	2.323	2.306	-	2.300	2.338

[1]Hedenbergite (Redhammer et al. 2006)
[2]High-temperature (1050 ºC) *C2/c* clinoferrosilite (Sueno et al. 1984).
[3]Fictive *C2/c* clinoferrosilite (Hugh-Jones et al. 1994), see text.

543

544
545

Table 6. Mössbauer parameters for synthetic clinopyroxenes.

Sample	QSD-site/ component	CS (mm/s)	QS (mm/s)	σ_{QS} (mm/s)	A_{QSD} (%)	A (%)	X_{Fe}^{2+}
$Hd_{50}Fs_{50}$	$^{M1}Fe^{2+}$	1.19(2)	2.23(5)	0.27	51(5)	35(4)	0.53(6)
	$^{M1'}Fe^{2+}$	1.18(2)	2.66(2)	0.12	49(5)	33(4)	0.50(6)
	$^{M2'}Fe^{2+}$	1.10(1)	1.77(1)	0.12	-	32(2)	0.48(3)
$Hd_{60}Fs_{40}$	$^{M1}Fe^{2+}$	1.19(2)	2.25(5)	0.28	61(5)	46(4)	0.64(6)
	$^{M1'}Fe^{2+}$	1.18(2)	2.69(2)	0.11	39(5)	29(4)	0.41(6)
	$^{M2'}Fe^{2+}$	1.10(1)	1.80(1)	0.10	-	25(2)	0.35(3)
$Hd_{70}Fs_{30}$	$^{M1}Fe^{2+}$	1.19(2)	2.24(5)	0.29	74(5)	60(4)	0.78(5)
	$^{M1'}Fe^{2+}$	1.18(2)	2.69(2)	0.11	26(5)	21(4)	0.27(5)
	$^{M2'}Fe^{2+}$	1.10(1)	1.82(1)	0.10	-	19(2)	0.25(3)

For the QSD site of Fe^{2+} at M1, the centre shift (CS) is linearly coupled to the quadrupole splitting (QS) by the relation: $CS = \delta_0 + \delta_1 QS$, where δ_1 is the coupling parameter. σ_{QS} = Gaussian width of the QSD, A_{QSD} = relative proportions of the two components of the QSD for Fe^{2+} at M1, A = relative area for a specific Fe site. $X_{Fe}^{2+} = Fe^{2+}$ occupancy.

546
547

548
549
550

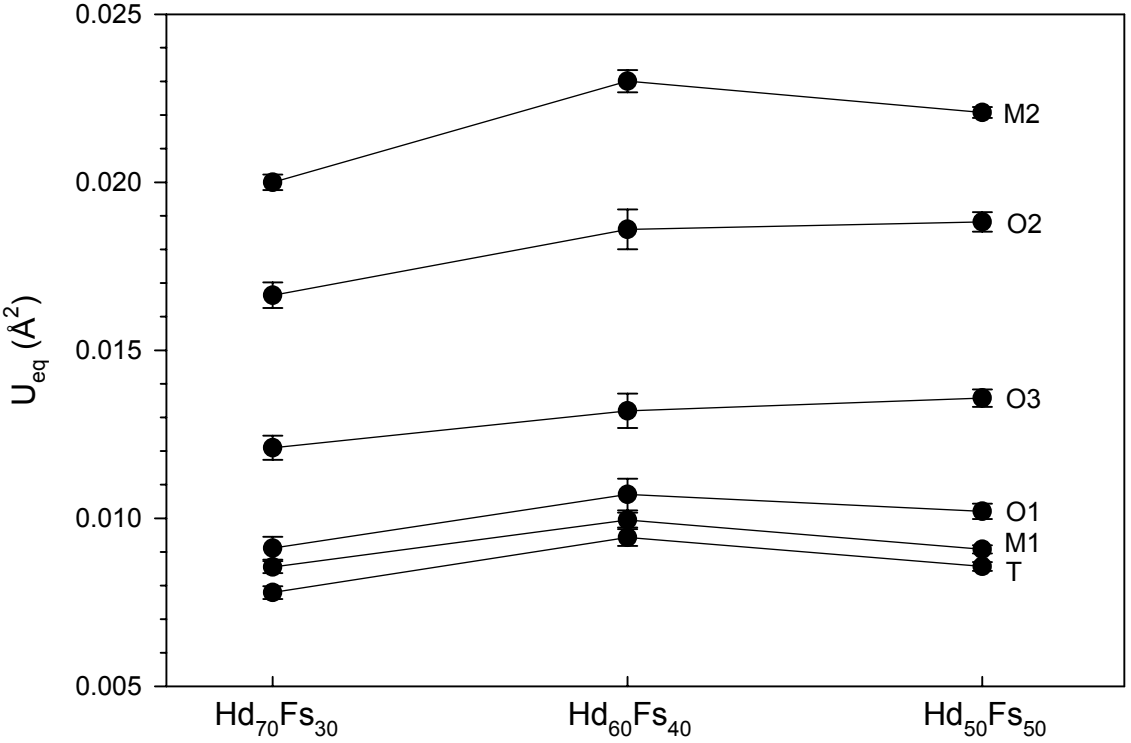

551
552
553
554 Fig. 1
555

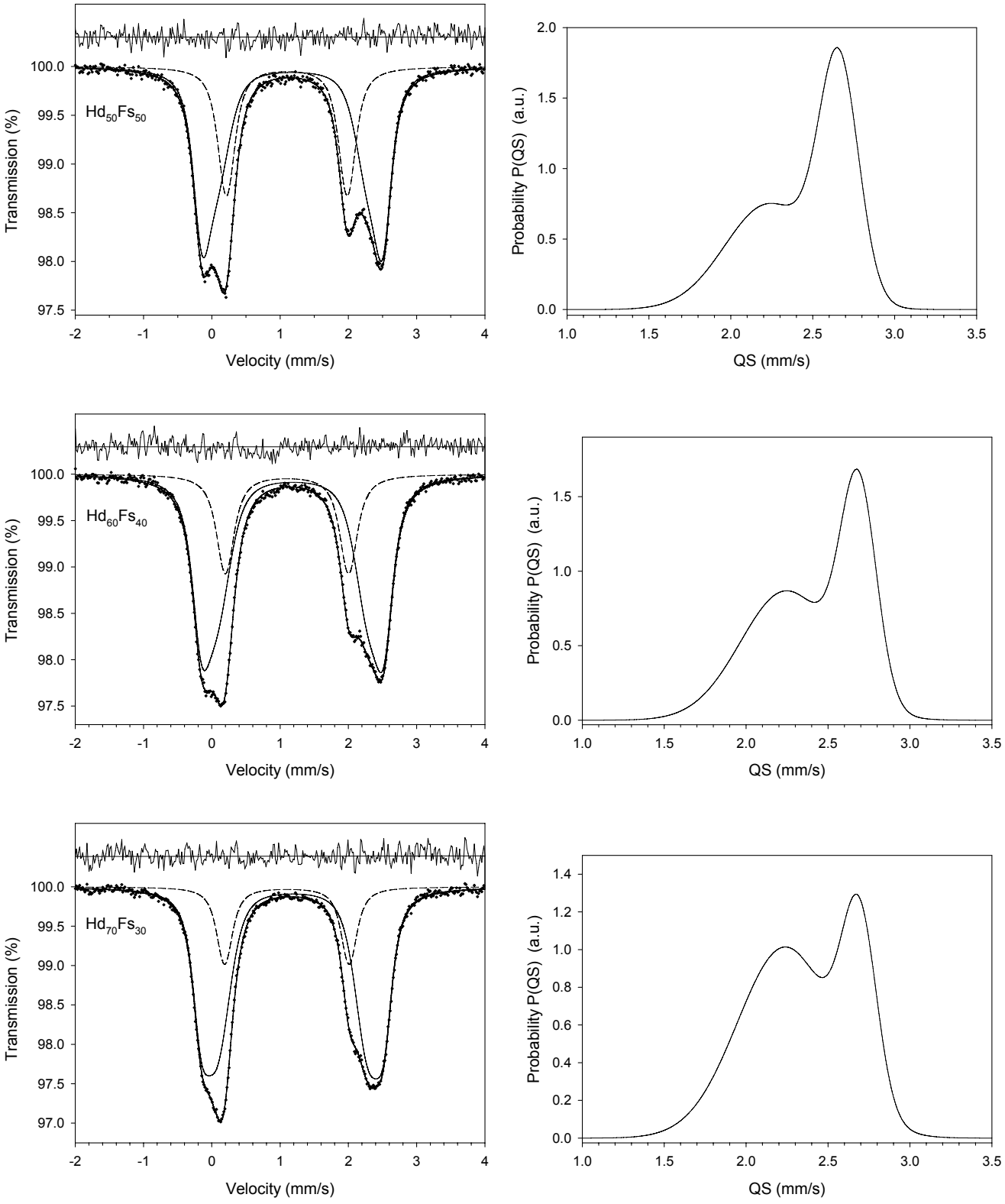

Fig. 2

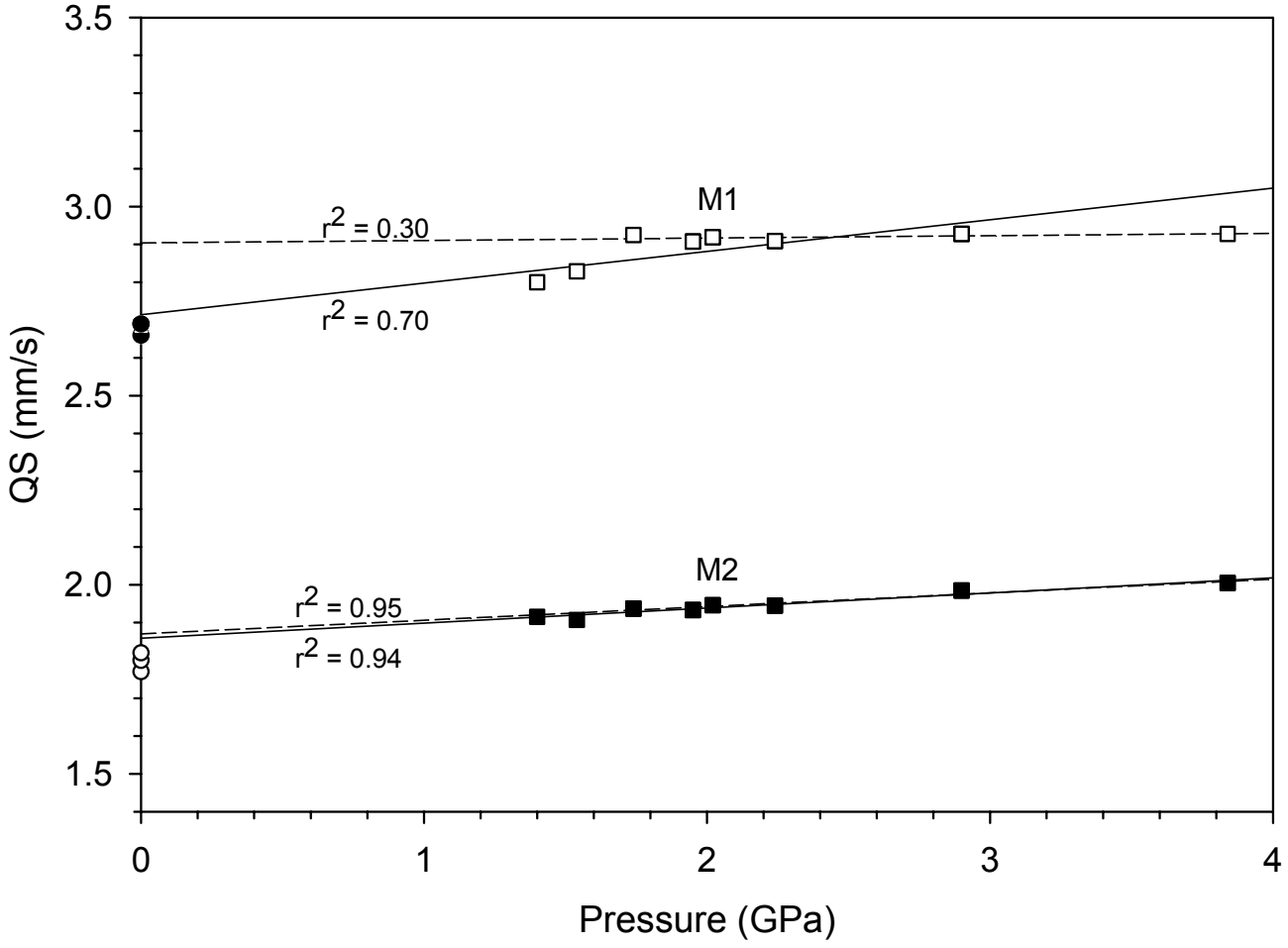

Fig. 3

572
573
574
575

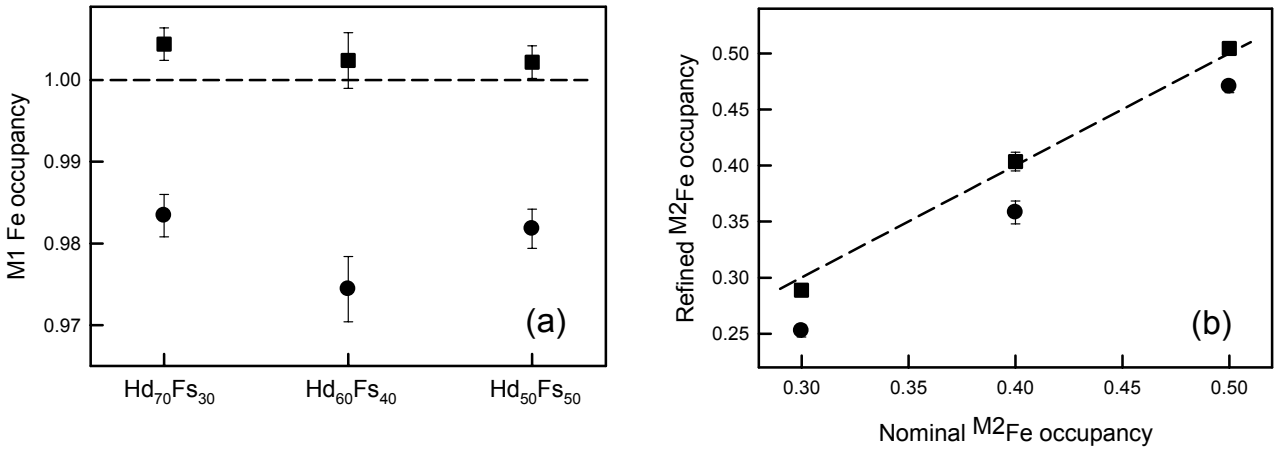

576
577
578
579
580
581 Fig. 4